Soft computing model for analysing the effect of friction stir processing parameters on the intergranular corrosion susceptibility of aluminium alloy AA5083

Výpočetní model pro analýzu vlivu paramatrů frikčního svařování na náchylnost k mezikrystalové korozi hliníkové slitiny AA5083

Vaira Vignesh R.[1], Padmanaban R.[1], Chinnaraj K.[2]
[1] Department of Mechanical Engineering, Amrita School of Engineering, Coimbatore, Amrita Vishwa Vidyapeetham, India
[2] Ashok Leyland Technical Center, Chennai
E-mail: dr_padmanaban@cb.amrita.edu

Aluminium alloy AA5083 is prone to intergranular corrosion in marine environments. In an attempt to reduce the intergranular corrosion, AA5083 was subjected to friction stir processing (FSP). The FSP experimental trials were conducted as per face-centered central composite design with three levels of variation in FSP process parameters viz. tool rotation speed (TRS), tool traverse speed (TTS) and tool shoulder diameter (SD). Intergranular corrosion susceptibility of the processed specimens was assessed by performing nitric acid mass loss test. The mass loss of the specimens was correlated with the intergranular corrosion susceptibility as per the standard ASTM G67-13. The experimental results indicate that FSP had significantly reduced the intergranular corrosion susceptibility of the AA5083 alloy. Soft computing techniques namely Artificial Neural Network, Mamdani Fuzzy system, and Sugeno Fuzzy system were used to predict the intergranular corrosion (IGC) susceptibility (mass loss) of the friction stir processed specimens. Among the developed models, Sugeno fuzzy system displayed minimum percentage error in prediction. So Sugeno fuzzy system was used to analyze the effect of friction stir processing process parameters on the IGC of the processed specimens. The results suggest that stir processing of AA5083 at a TRS of 1300 rpm, TTS of 60 mm/min and SD of 21 mm would make the alloy least susceptible to intergranular corrosion.

Hliníková slitina AA5083 je náchylná k mezikrystalové korozi (MKK) v mořském prostředí. Slitina AA5083 byla v rámci pokusu o potlačení vlivu mezikrystalové koroze podrobena frikčnímu svařování (FSP). Svařovací zkoušky proběhly na zařízení s třemi ovladatelnými parametry: rychlost rotace (TRS), pohyb nástroje (TTS) a průměr nástroje (SD). Náchylnost k MKK byla ověřována pomocí testu hmotnostních úbytků v roztoku kyseliny dusičné podle normy ASTM G67-13. Výsledky experimentů ukazují, že frikční svařování výrazně snižuje náchylnost k MKK. K predikci náchylnosti k MKK byly použity výpočtové metody: neuronová síť, Mamdaniho porces a Sugeno proces. Sugebno porces vykazuje nejvyšší přesnost pro predikci náchylnosti k MKK. Byly nalezeny optimální podmínky svařování: TRS 1300 rpm, TTS 60 mm/min y SD 21 mm.

INTRODUCTION

Ultra-pure aluminum has high corrosion resistance [1]. The 5xxx series of aluminum alloys are Al-Mg based alloy systems and specifically, AA5083 is used in the construction of ships and boats, due to its good corrosion resistance [2]. The microstructure of AA5083 consists of primary phase (α–Al) and secondary phase (β–Mg_3Al_2). The precipitation of β phase over a period of time increases the intergranular corrosion (IGC) susceptibility of this alloy. Interphase galvanic corrosion is induced in the alloy as β phase exhibits anodic potential with respect to α phase [3]. Precipitation of β phase as continuous network promotes intergranular stress corrosion cracking [4] and IGC [5] in AA5083.

From the literature [3-5], it is professed that precipitation, agglomeration or continuous network of β phase results in intergranular corrosion of the matrix. So corrosion rate of AA5083 can be controlled by disintegrating and/or dispersing β phase, which can be achieved by alloying or heat treatment process.

Corrosion being a surface phenomenon can also be controlled by surface modification and coating processes. Friction stir processing (FSP) is one of the solid-state surface and subsurface modification processes, in which the composition of the matrix remains un-altered post-processing. FSP is similar to the friction stir welding process, in which a rotating tool is traversed along the length of the plate in the processing direction under the action of an axial load. The microstructural refinement in

FSP is similar to that of friction stir welding [6] and the schematic of FSP is shown in Figure 1.

Mishra et al., [7] found that the properties of friction stir processed materials are dependent on various process parameters such as tool rotation speed, tool traverse speed, axial force [8], geometric profile of tool (shoulder diameter, pin diameter, pin profile), and backing plate temperature [9]. Ma [10] reviewed the effect of FSP process parameters on the microstructural refinement of the metals and alloys. Padmanaban et al., [11] studied the effect of friction stir spot welding process parameters on the tensile strength of friction stir spot welded AA6061 joints.

Recently, artificial intelligence systems are gaining momentum in the field of intelligent manufacturing, process control, smart computation, complex decision analysis systems and design optimization [12-14]. The development of artificial intelligence systems is catego-rized as expert systems and artificial neural network systems. The expert systems are knowledge-based systems, in which the problems are solved or conclusions are drawn based on the set of rules given by the user. The processing style of such expert systems follows a sequence. Fuzzy systems are examples of expert systems. Artificial neural network (ANN) is a biologically inspired computer program developed to process data and its functioning is analogous to the human brain. ANN is trained through experience and not based on the programming codes or set of rules. ANN gains knowledge by sensing the patterns and relationships in the data.

In this study, two soft computing techniques (ANN and Fuzzy) were used to predict the IGC susceptibility of AA5083. In fuzzy soft computing approach, the prediction efficiency of Mamdani and Sugeno based inference methods were analyzed. The prediction efficiency of the models generated by ANN, Mamdani fuzzy system, and Sugeno fuzzy system was compared and the model with the least prediction error was chosen for studying the effect of FSP process parameters on the IGC susceptibility of AA5083 alloy. As Sugeno based fuzzy system exhibited the least percentage error in prediction, it was used to analyze the effect of process parameters on the IGC susceptibility of friction stir processed (FSPed) AA5083.

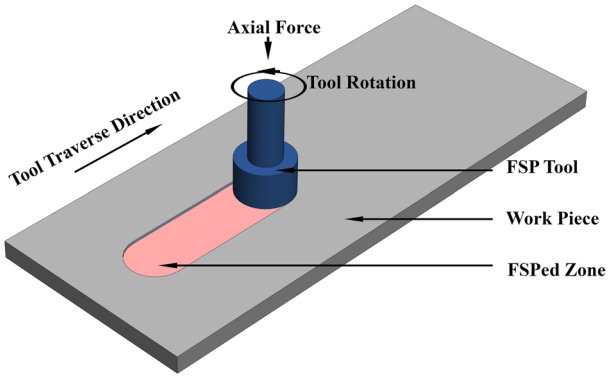

Fig 1. Schematic of friction stir processing
Obr. 1. Schéma procesu frikčního svařování

MATERIALS AND METHODS

Materials

Wrought aluminum alloy AA5083 of dimension 150 mm × 60 mm × 5 mm were used in the study. The nominal composition of the alloy is given in Table 1.

Tab. 1. Nominal composition of AA5083 / *Složení slitiny*

El	Mg	Mn	Si	Fe	Zn	Cu	Cr	Al
Wt.%	4.7	0.5	0.11	0.29	0.08	0.05	0.08	Rest

Design of Experiments

Face-centered central composite design (FC-CCD) is a widely used experimental design in statistics to establish a relationship between the input process parameters and the output result, with a minimum number of experimental trials. FC-CCD is advantageous over conventional factorial designs, as it has center points augmented with the axial points in the design cube. This increases the prediction efficiency of the model developed through FC-CCD. In this study, three FSP process parameters were varied at three levels. The chosen parameters and their levels are given in Table 2.

Tab. 2. Chosen level of process parameters and their corresponding levels / *Vybrané úrovně procesních parametrů*

Sl.	FSP process parameters			Linguistic term
	TRS (rpm)	TTS (mm/min)	SD (mm)	
1	700	30	15	L
2	1000	45	18	M
3	1300	60	21	H

Friction stir processing

The workpieces were cleaned and degreased with acetone before FSP trials. The workpieces were FSPed in a numerically controlled vertical milling machine. FSP tool was plunged into the workpiece and after a dwell time of 60 seconds, FSP trials were performed as per the FC-CCD experimental layout.

Intergranular corrosion susceptibility test

Intergranular corrosion susceptibility of AA 5083 was assessed by conducting nitric acid mass

loss test according to the ASTM standard. The FSPed workpieces were cut into specimens of length 40 mm. A metallographic emery sheet of 300 grit was used to smoothen the edges of the specimen. The dimensions of the specimens were measured using a Mitutoyo make digital vernier caliper. The surface area of the specimen (A) was estimated using (1), where the dimensions of the specimen are denoted as length (L), breadth (B) and height (H).

$$A = 2 \cdot [(L \cdot B) + (B \cdot H) + (L \cdot H)] \quad (1)$$

The specimens were desmutted by immersing in 5% sodium hydroxide (NaOH) at 80°C for one minute, followed by rinsing in distilled water. Then the specimens were immersed in concentrated nitric acid (HNO_3) for thirty seconds. The specimens were rinsed in distilled water and dried in hot air. The specimens were weighed using a Shimadzu make weighing balance with a readability of 0.0001 g. The specimens were placed in a glass container such that their edges rest against the walls of the container. As outlined by ASTM standard, concentrated HNO_3 was filled in the container maintaining acid volume to specimen surface area ratio at 30000 ml.m^{-2}. The specimens were completely immersed and left undisturbed in the glass container for a time period of 24 hours. After the immersion period, the specimens were removed and rinsed in distilled water. The corrosion products and any particles adhering over the surface of the specimens were removed using a stiff plastic brush, followed by rinsing in cold water. The specimens were dried in a blast of hot air and weighed in the weighing balance. The mass loss of the specimens per unit area (M_a) was calculated using (2).

$$M_a = \frac{\Delta m = (m_1 - m_2)}{A} \quad [\text{mg}\cdot\text{cm}^{-2}] \quad (2)$$

where m_1 denotes the mass of specimen after desmutting process; m_2 denotes mass of specimen post IGC susceptibility test.

The surface morphology of the specimens was characterized by a field emission – scanning electron microscope (FE-SEM). The FE-SEM (Make: Carl Zeiss) images were captured at an accelerating voltage (electron high tension EHT) of 10 kV.

Artificial neural network

ANN model has functionalities similar to the information processing modules of the human brain [15]. ANN is used to handle complex mathematical tasks such as fitting complex models, classification of complex data or signals, data clustering and time series forecasting [16]. ANN is a computational model developed by interconnecting the artificial neurons with the weights (coefficients) which constitutes the neural network. Artificial neurons are also called as processing elements, as they have weighted inputs, transfer function, and one output. Certain simple functions can be processed by a single neuron in the network. The power of ANN computations increases, as the number of neurons in the network is increased. In this study, a feedforward architecture based ANN model was constructed as shown in Figure 2. The learning algorithm used was Levenberg Marquardt algorithm.

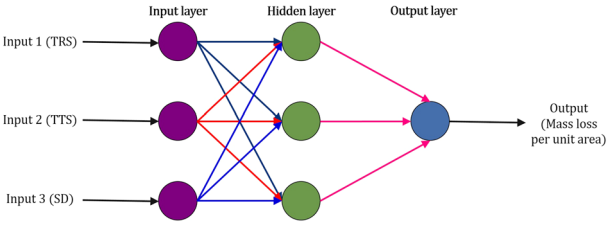

Fig. 2. Layout of artificial neural network
Obr. 2. Schéma neuronové sítě

Levenberg Marquardt (LM) algorithm is one of the efficient supervised learning algorithms, in which the learning rate ε is set to unity and an additional term e^{λ} is introduced in the second derivative error. Let us consider a second order function $F(w)$, g be its gradient vector and $[H]$ be its Hessian matrix. In LM algorithm, an optimum adjustment in the weight vector (w) is given according to (3).

$$\Delta w = [H + \lambda I]^{-1}\, g \quad (3)$$

where Δw is optimum adjustment applied for w, I is identity matrix with dimensions as $[H]$ and λ is regularizing parameter that forces $[H + \lambda I]$ to be positive definite. The feedforward network with single output neuron network is trained by minimizing the cost function which is given by (4).

$$\xi_{av} = \frac{1}{2N} \sum_{i=1}^{N} [d(i) - F(x(i);w)]^2 \quad (4)$$

where $\{x(i), d(i)\}_{i=1}^{N}$ is the training data set consisting of inputs and outputs, $F(x(i);w)$ is the approximating function. The gradient and approximated Hessian of ξ_{av} is given by the (5) and (6) respectively.

$$g(w) = \frac{\partial \xi_{av}(w)}{\partial w} = \frac{-1}{N} \sum_{i=1}^{N} [d(i) - F(x(i);w)]^2 \frac{\partial F(x(i);w)}{\partial w} \quad (5)$$

$$H(w) \approx \frac{-1}{N} \sum_{i=1}^{N} \left[\frac{\partial F(x(i);w)}{\partial w}\right] \left[\frac{\partial F(x(i);w)}{\partial w}\right]^{T} \quad (6)$$

In this method, λ is chosen automatically (starting from a value), until a downhill step is produced for each epoch. This reduces the error in the predictions made using the developed ANN model. The training of network terminates prior to the number of specified epochs if the conditions given in (7) and (8) are reached.

$$\lambda = 10 \cdot \Delta\lambda + \text{Max}\,[H] \quad (7)$$

$$\frac{MSE_{w_m} - MSE_{w_{m+1}}}{MSE_{w_m}} \leq MSE_{min} \quad (8)$$

where MSE is mean squared error.

Fuzzy logic method

Fuzzy logic sets provide means to model the relationship between the input process parameters and output, even for problems with the uncertainty associated with vagueness and imprecision [17]. The schematic of a fuzzy system is shown in Figure 3.

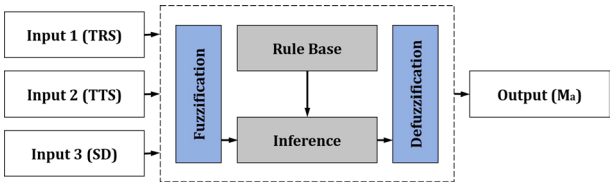

Fig. 3. Schematic of fuzzy system
Obr. 3. Schéma fuzzy systému

Membership functions take a value between 0 and 1 and map the membership value with the input space. Gaussian membership function ensures smooth boundary conditions for invoking the fuzzy rules [18] and hence used in this study. The input parameters (either analog or digital) are translated to linguistic quantities, associated with the membership function and then subjected to fuzzification. The process of comparing the input parameters with the membership function and obtaining membership value for each linguistic quantity is known as fuzzification. The translated data is applied to the predefined set of rules in the rule base in the inference mechanism. The inference mechanism generates output in the form linguistic terms. These terms are again converted to crisp function or value by defuzzification process [18]. The major inference methods in the fuzzy logic system are Mamdani's fuzzy inference method and Sugeno fuzzy inference method. Mamdani fuzzy system uses fuzzy sets as rule consequent whereas Sugeno fuzzy system uses linear functions of input variables as rule consequent [19].

RESULTS

Artificial Neural Network model

In this study, a multilayer perceptron network (MLP) consisting of three layers of neurons was used. The first layer of neurons was the input layer, the intermediate layer was the hidden layer and the third layer was the output layer of neurons. In general, the stages in MLP model with p input neurons, q hidden neurons, and r output neurons are constructed as given below. The input layer of neurons is mapped with the hidden layer of neurons by using the (9) and (10).

$$u_j = w_{oj} \sum_{i=1}^{n} w_{ij} \cdot x_i \quad (9)$$

$$y_j = f(u_j) \quad (10)$$

where i and j are number of neurons in the input layer and hidden layer respectively, x_i is the i^{th} input, w_{ij} is the weight associated with the input i and the neuron j, w_{oj} is the bias weight of the hidden neuron j and $f(u_j)$ is the activation function of the j^{th} neuron that transfoms any hidden neuron input u_j to hidden neuron output y_j. The hidden layer neurons are mapped with the output layer of neurons using the (11) and (12).

$$w_k = w_{ok} \sum_{j=1}^{m} w_{jk} \cdot y_j \quad (11)$$

$$z_k = f(v_k) \quad (12)$$

where m and k are number of neurons in hidden layer and output layer respectively, y_j is the j^{th} output, w_{jk} is the weight related with the output k and the neuron j, w_{ok} is the bias weight of output neuron and $f(v_k)$ is the activation function of the k^{th} neuron that transforms any weighted sum of inputs v_k to the final output z_k. Equation (13) is used to calculate the MSE for all the training pattern of the networks with only one output neuron.

$$MSE = \frac{1}{N} \sum_{i=1}^{N} (t_i - z_i)\ \text{^}2 \quad (13)$$

where N is the number of training patterns, t_i is the target value and z_i is the predicted value.

The technical computing environment MATLAB R2015© was used to generate the ANN model. The FSP process parameters were the inputs and M_a was the

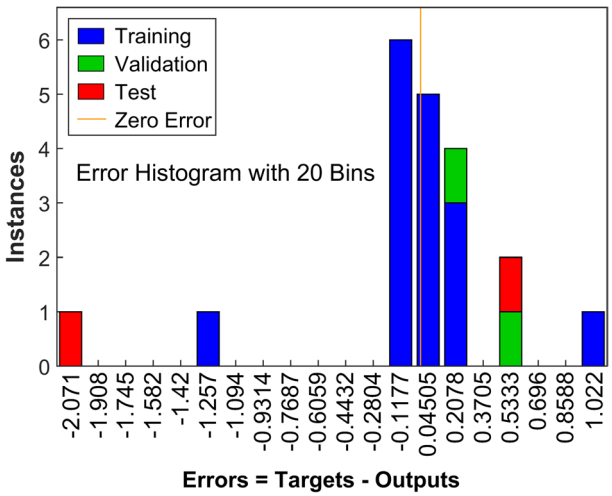

Fig. 4. Error histogram of ANN model
Obr. 4. Chybový histogram modelu neuronové sítě

out-put. In this study, ANN was constructed with three neurons in the input layer, two neurons in the hidden layer and one neuron in the output layer. 80% of the experimental data was used for training and remaining 20% of the data was used for validation and testing. LM algorithm was used to train the neural network model until the correlation coefficient (R) was maximum and MSE was minimum. Figure 4 shows the error histogram for the ANN predicted values.

The experimental versus predicted values of the training set, testing set, and validation set is shown in the Figure 5. A non-linear trend was observed between the experimental and predicted values. The correlation coefficients for training data, validation data and checking data were found to be 0.86802, 1 and 1 respectively. The overall correlation coefficient for the ANN model was found to be 0.7651. The overall correlation coefficient was not close to one, indicating inefficiency of the model in predicting the output.

Mamdani fuzzy system model

Mamdani fuzzy system for predicting the M_a of the FSPed specimens was generated using MATLAB. The lower level of the FSP process parameters (input) was coded as 'L', middle level as 'M' and high level as 'H' as given in Table 2.

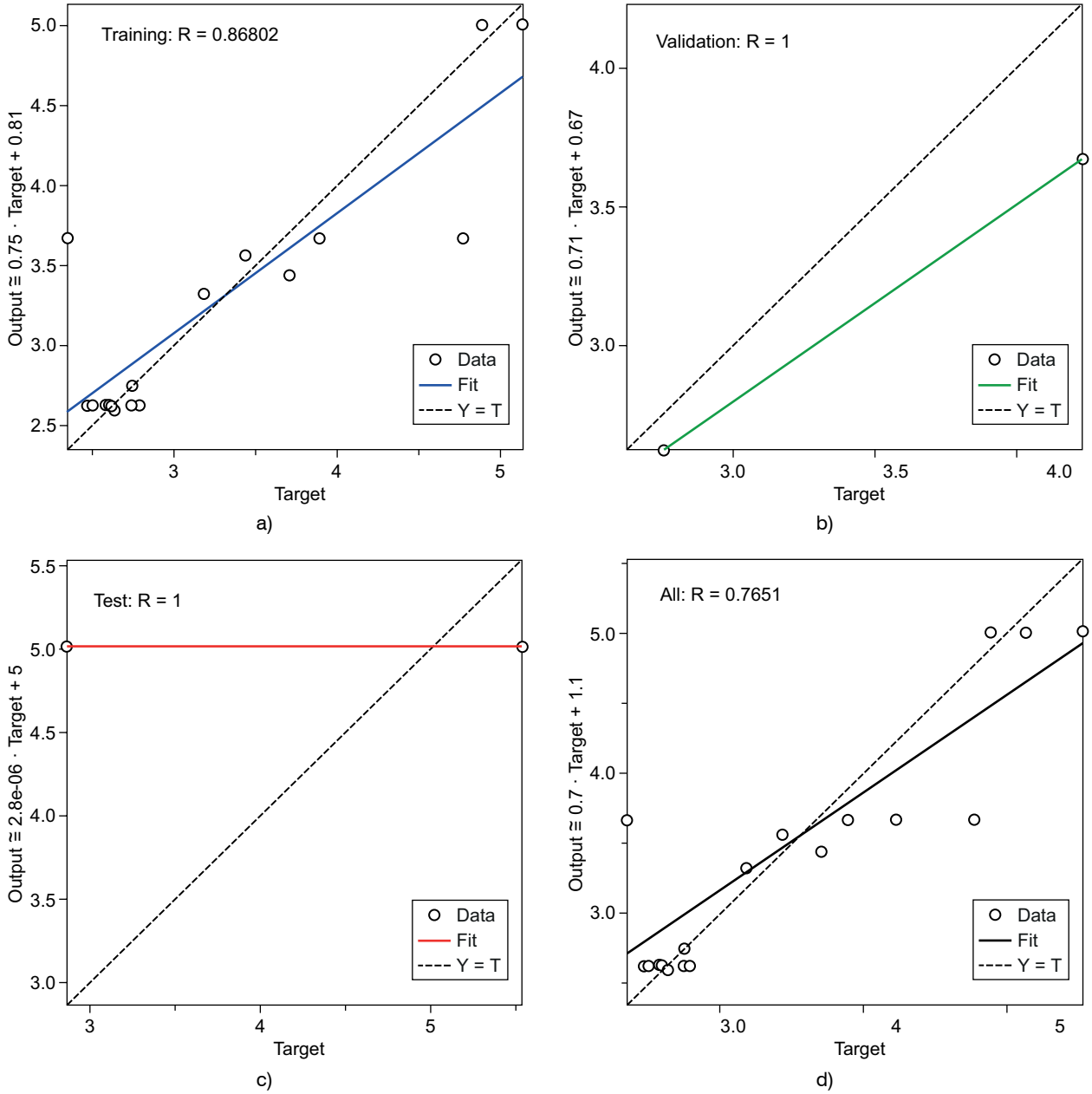

Fig. 5. Experimental vs predicted values of: a) Training data; b) Validation data; c) Test data; d) Overall data
Obr. 5. Experimentální vs. predikovaná data

The M_a (output) is categorized into 17 ranges and their corresponding coded variables are given in Table 3. The fuzzy logic layout is shown in Figure 6a. As discussed earlier, Gaussian membership function was associated with each level in the input and each range in the output. The membership functions for TRS, TTS, SD, and M_a are shown in Figures 6b-e respectively.

Tab. 3. Coded variable for the chosen range of M_a / *Vybrané proměnné pro testování*

Sl.	Mass loss per unit area (mg cm^{-2})		Coded variable
	Lower limit	Upper limit	
1	2.30	2.5	M1
2	2.51	2.70	M2
3	2.71	2.90	M3
4	2.91	3.10	M4
5	3.11	3.30	M5
6	3.31	3.50	M6
7	3.51	3.70	M7
8	3.71	3.90	M8
9	3.91	4.10	M9
10	4.11	4.30	M10
11	4.31	4.50	M11
12	4.51	4.70	M12
13	4.71	4.90	M13
14	4.91	5.10	M14
15	5.11	5.30	M15
16	5.31	5.50	M16
17	5.31	5.54	M17

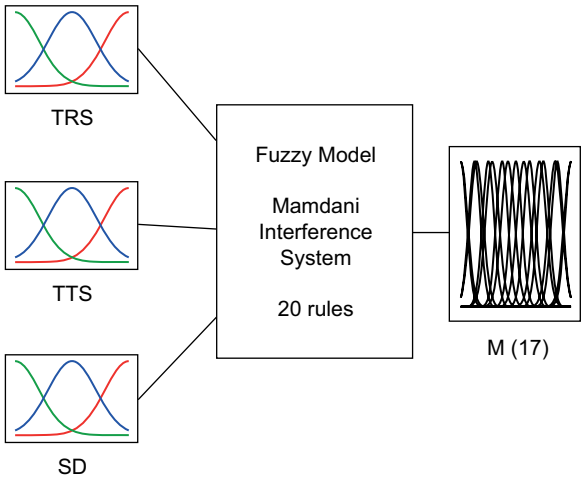

a)

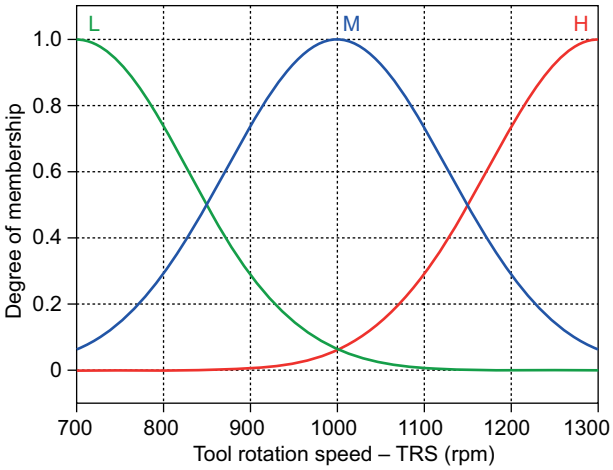

b)

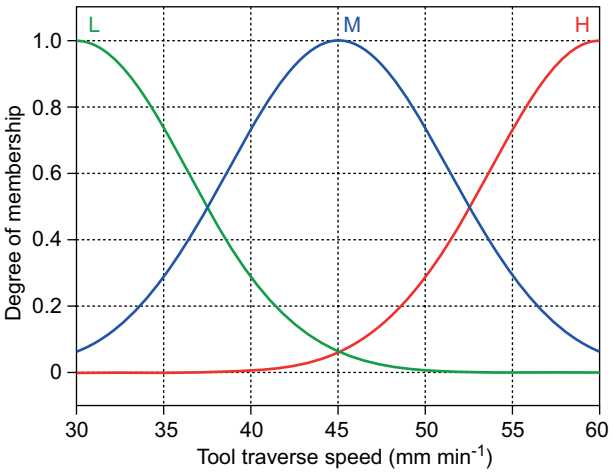

c)

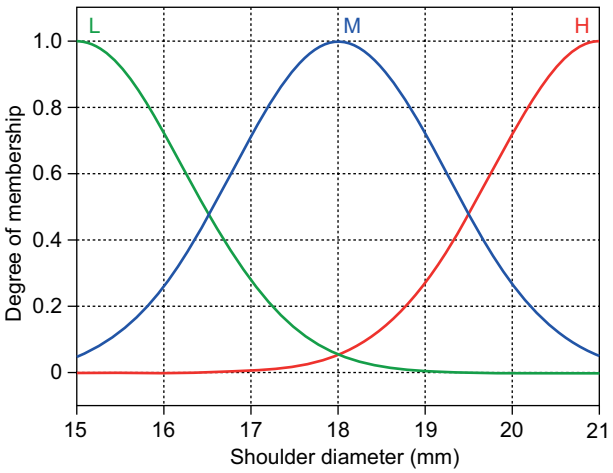

d)

Fig. 6. Layout of Mamdani fuzzy system (a); Membership function for TRS (b); Membership function for TTS (c); Membership function for SD (d) – *Continue on next page*
Obr. 6. Schéma Mamadani procesu – Pokračování na další stránce

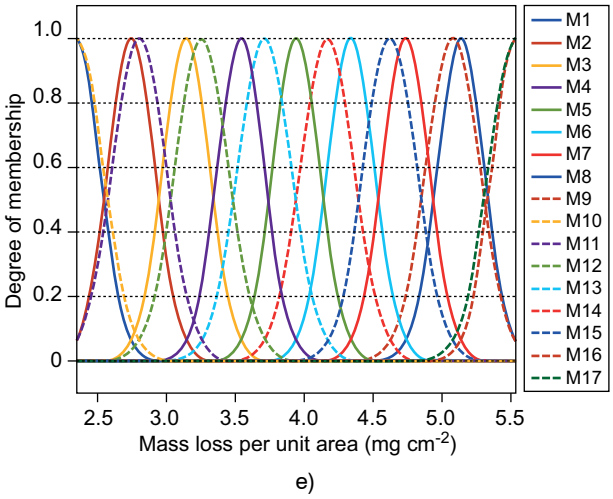

e)

Fig. 6. Membership function for M_a (e)
Obr. 6. Schéma Mamadani procesu

Tab. 4. Experimental results mass loss per unit area M_a / *Experimentální výsledky hmotnostních úbytků*

Sl.	TRS (rpm)	TTS (mm/min)	SD (mm)	Experimental mass loss per unit area, M_a (mg cm^{-2})
1	700	30	15	5.534
2	1300	30	15	3.435
3	700	60	15	2.864
4	1300	60	15	4.232
5	700	30	21	3.183
6	1300	30	21	4.774
7	700	60	21	2.639
8	1300	60	21	2.347
9	1000	45	18	2.605
10	1000	45	18	2.738
11	1000	45	18	2.754
12	1000	45	18	2.468
13	700	45	18	5.135
14	1300	45	18	3.896
15	1000	30	18	3.706
16	1000	60	18	2.749
17	1000	45	15	4.887
18	1000	45	21	2.582
19	1000	45	18	2.505
20	1000	45	18	2.785

The rule consequent (rule base) with three parameters p_1, p_2 and p_3 as input and one parameter q as output is given below.

Rule 1: If p_1 is D_1, p_2 is E_1 and p_3 is F_1, then q is $f_1(x)$
Rule 2: If p_1 is D_2, p_2 is E_2 and p_3 is F_2, then q is $f_2(x)$
….
Rule n: If p_1 is D_n, p_2 is E_n and p_3 is F_n, then q is $f_n(x)$

where D_i, E_i, and C_i are subsets defined by analogous membership functions and $f_i(x)$ is the crisp function. The set of 20 rules are framed on the basis of membership functions of the input and output variables. The model was used to predict the M_a for the input data. The percentage error in prediction was calculated using (14).

$$\% \, Error = \left(1 - \frac{\text{Predicted value}}{\text{Experimental value}}\right) \cdot 100 \qquad (14)$$

Sugeno fuzzy system model

The layout of Sugeno fuzzy system is shown in Figure 7a. The input process parameters were associated with the Gaussian membership function. In this study, fuzzy inference system was trained by a hybrid neuro-fuzzy system. In Sugeno fuzzy system, defuzzification is done by adaptive neuro-fuzzy interference system (ANFIS).

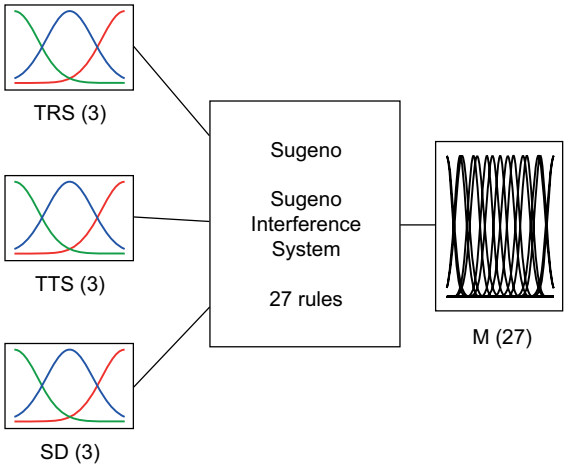

a)

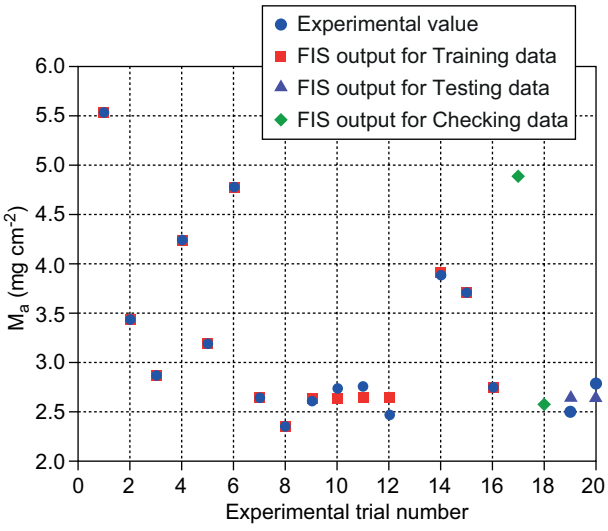

b)

Fig. 7. Layout of Sugeno fuzzy system (a); Training data, Test data and Checking data and corresponding FIS Output (b)
Obr. 7. Schéma Sugeno procesu

As this study had three FSP process parameters (input) and each process parameter was varied at three levels, 27 rules were generated in the ANFIS structure.

The number of epochs and error tolerance were given as 6 and 0 respectively. 80% of the experimental data was used for training, 10 % of the experimental data was used for testing and the remaining 10% of the experimental data was used for checking. The training data, testing data and checking data and their corresponding FIS output is shown in Figure 7b. The model was used to predict the M_a.

DISCUSSIONS

The mass loss per unit area of the friction stir processed AA5083 are given in Table 4. The percentage error in prediction between the experimental and predicted values are given in Table 4. Figure 8 depicts the error in prediction of M_a, made by ANN model, Mamdani fuzzy system model, and Sugeno fuzzy system model.

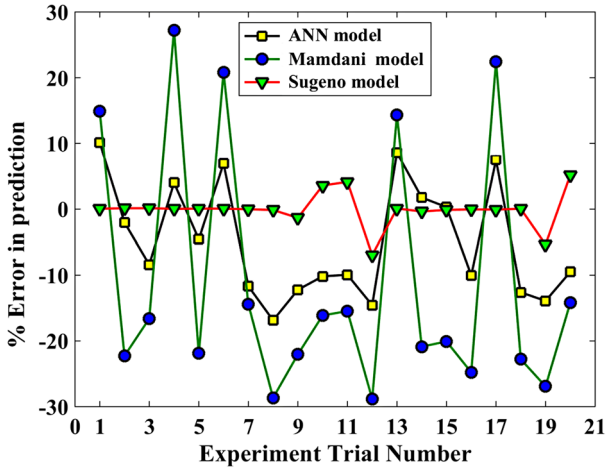

Fig. 8. Percentage error in prediction for ANN, Mamdani and Sugeno models
Obr. 8. Procentuální chyby modelů

The percentage error in prediction ranged between -30% and +30% in the Mamdani fuzzy system model. The range of percentage error in prediction for ANN model was between -20% and +10%. Comparing the ANN model and Mamdani fuzzy system model prediction efficiency, the latter had the least accuracy in prediction. It is observed from the figure that the Sugeno fuzzy system model had the highest efficiency in prediction, as percentage error in prediction did not exceed 10% for all observations. So Sugeno fuzzy system model was considered to analyze the effect of FSP process parameters on the IGC susceptibility of FSPed specimens.

Surface morphology analysis

AA5083 consists of primary phase (α–Al) and secondary phase (β–Al_2Mg_3) in the matrix [20]. An intermediate mass loss of 19.967 mg cm^{-2} was observed for the base material. In the course of IGC susceptibility test, HNO_3 dissolved the secondary phase in preferential to the solid solution of Mg in the alloy matrix. This depleted β phase present in the grain and along the grain boundaries, which resulted in loosening and falling of α phase grains from the matrix. It caused a huge mass loss in the order of 15 to 25 mg cm^{-2}, as outlined by the ASTM standard G67-13.

As seen in Figure 9a, the microstructure of the base specimen subjected to IGC test displays pits and corroded grains. H_2 gas from concentrated HNO_3 diffused into alloy matrix through the notch root regions on the surface. Trapping and subsequent release of H_2 gas resulted in intergranular corrosion [21]. The segregation of Mg

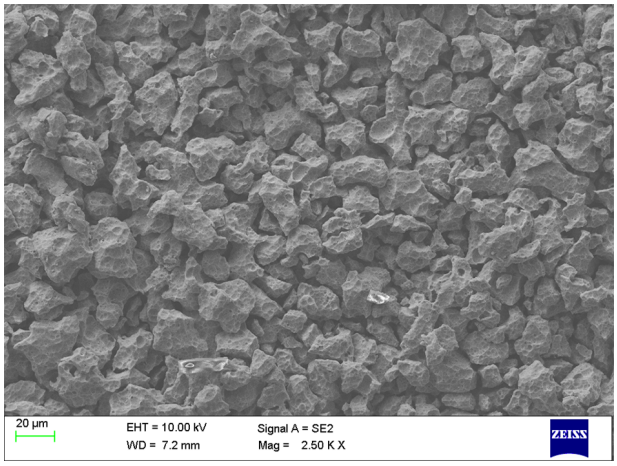

a)

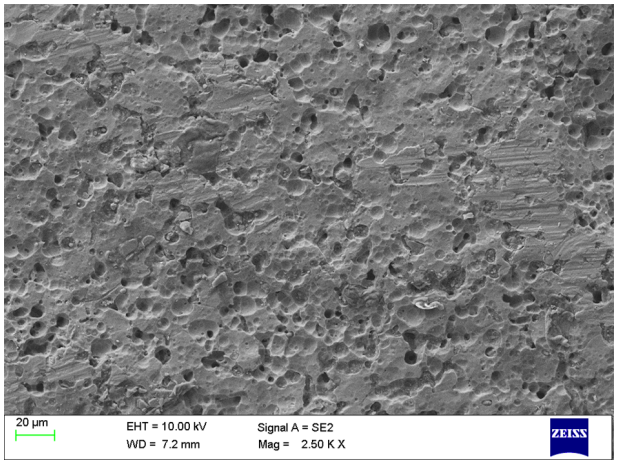

b)

Fig. 9. FESEM image of base specimen post IGC test and FSPed specimen FSP08 post IGC test (b)
Obr. 9. Obrázek z elektronového mikroskopu (základní materiál a vzorek po svařování)

towards the grain boundary and/or formation of coarse precipitates of β phase inducted hydrogen embrittlement in the matrix by forming hydrides or by hydrogen chemisorption [22]. Added to this phenomenon, galvanic coupled corrosion was induced between the noble α phase [23, 24] and active β phase [3].

The FSPed specimens were lesser prone to intergranular corrosion, as it is evident from lower mass loss (< 15 mg cm^{-2}) than the base material. The phase diagram of Al–Mg alloy system is shown in Figure 10 and it is observed that Al_2Mg_3 precipitates at a temperature of 683 K. The nominal plasticizing temperature obtained during FSP is 400°C (approximately) [11, 25]. The heat generation and strain developed during FSP causes recovery, recrystallization and grain growth in the neighborhood of the processing zone. During FSP, the region in front and behind of FSP tool undergo static recovery – static recrystallization. The processing region beneath FSP tool undergoes dynamic recovery and dynamic recrystallization [6]. During this process, the formation of β phase in the grains restricted the motion of Mg towards the grain boundary [26] and it resulted in finely dispersed secondary phases in the matrix [27]. This reduced the availability of β phase for dissolution by HNO_3. Hydrogen embrittlement was also reduced, as the β phase is a preferential site for H_2 storage. This consequently reduced the intergranular corrosion of FSPed specimens [24, 28]. FE-SEM image of the FSP08 specimen after IGC susceptibility test shown in Figure 9b displays intact grains and a few pits. The recovery and recrystallization phenomenon are dependent on the strain and thermal cycles during FSP. As the process parameters influence the thermal cycles, thermal analysis during FSP is discussed in the following section.

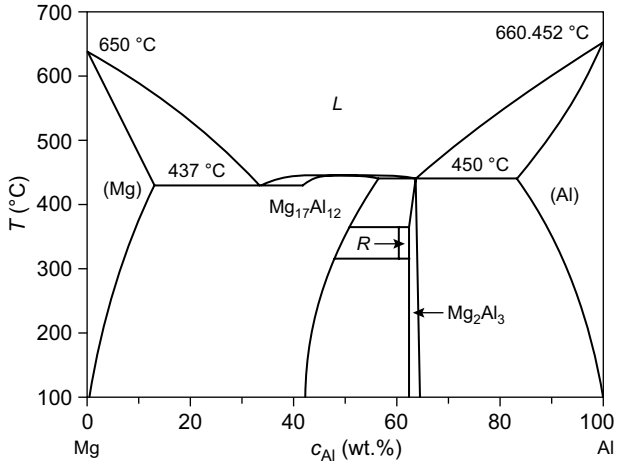

Fig. 10. Binary phase diagram of aluminum-magnesium alloy system [22]
Obr. 10. Binární diagram Al–Mg

Thermal analysis during FSP

The governing equation for heat transfer during FSP is given by (15). The heat generated at the shoulder – workpiece and tool pin – workpiece interfaces are given by (16) and (17) respectively. The relation between the angular velocity and TRS is given by (18). From (15) to (18), it is observed that the peak temperature reached during FSP is reliant on the TRS, TTS, and SD [9].

$$\rho\, C_p\, u \cdot \nabla T + \nabla \cdot (-k \nabla T) = Q \tag{15}$$

$$q_{\text{shoulder}} = \mu\, (F_n/A_s) \cdot \omega \cdot r_s \tag{16}$$

$$q_{pin} = \frac{\mu}{\sqrt{3(1+\mu)^2}} \cdot r_p \cdot \omega \cdot Y(T) \tag{17}$$

$$\omega = \frac{2\pi \cdot N}{60} \tag{18}$$

where ρ is density of material, u is TTS in m s^{-1}, N is TRS in rps, T is temperature in K, ω is angular velocity in rad/s, F_n is plunge force in N, r_p is pin radius in m, r_s is shoulder radius m, A_s is surface area of shoulder in m^2, μ is coefficient of friction, q_{pin} is heat generated at pin in W, q_{shoulder} is heat generated at shoulder in W and $Y(T)$ is average shear stress as a function of time F m^{-2}.

As it can be observed from (17) and (18), increase in angular velocity (which in turn dependent on TRS) increases the heat input to the workpiece. Consequently, a decrease in TRS decreases the amount of heat generated at the interface of the tool and the workpiece. It is evident from (15) that increase in TTS increases the rate of heat transfer. With the increase in TTS, the contact time between tool with the workpiece decreases, which decreases the heat input. From the (16), it is observed that heat generated at the tool-workpiece interface is proportional to the tool shoulder diameter. The frictional heat generated between the tool shoulder and the workpiece is greatly influenced by the surface area of contact between the tool and workpiece.

Interaction effects of FSP process parameters on M_a

The interaction effect of two FSP process parameter is analyzed through the surface plots. The effect of TRS and TTS on M_a is shown in Figure 11a. Specimens processed at high TRS of 1300 rpm and high TTS of 60 mm min^{-1} resulted in minimum M_a.

The insufficient heat generated at low TRS or high TTS resulted in the poor dynamic recovery and dynamic recrystallization. This resulted in non-uniform and coarse precipitates of β phase, which increased the M_a. It is observed from the Figure 11a that low TRS of 700 rpm and medium TTS of 45 mm/min resulted in M_a greater than M_a that occurred at other levels of TRS and TTS for SD of 18 mm. The effect of TRS and SD on M_a is shown

in Figure 11b and that variation of M_a due to variation of TRS at SD of 21 mm and variation of SD at TRS of 700 rpm and TRS of 1300 rpm follow a crest parabolic trend. The insufficient heat input at low TRS reduced the extent of recovery and recrystallization of the processed material. So the specimen processed at TRS of 700 rpm and SD = 18 mm resulted in more M_a than other interaction levels of TRS and SD for constant TTS of 45 mm/min. Figure 11c shows the interaction effect of TTS and SD on M_a. Crest parabolic trend is observed in M_a for the variation of TTS at an SD of 21 mm. Maximum M_a was observed in the specimen processed at medium TTS of 45 mm/min and SD of 21 mm. The variation of M_a with variation in SD at TTS of 30 mm/min follows a crest parabolic trend. But the peak point of this parabolic curve was observed to be smaller than the former curves Figures 11a,b.

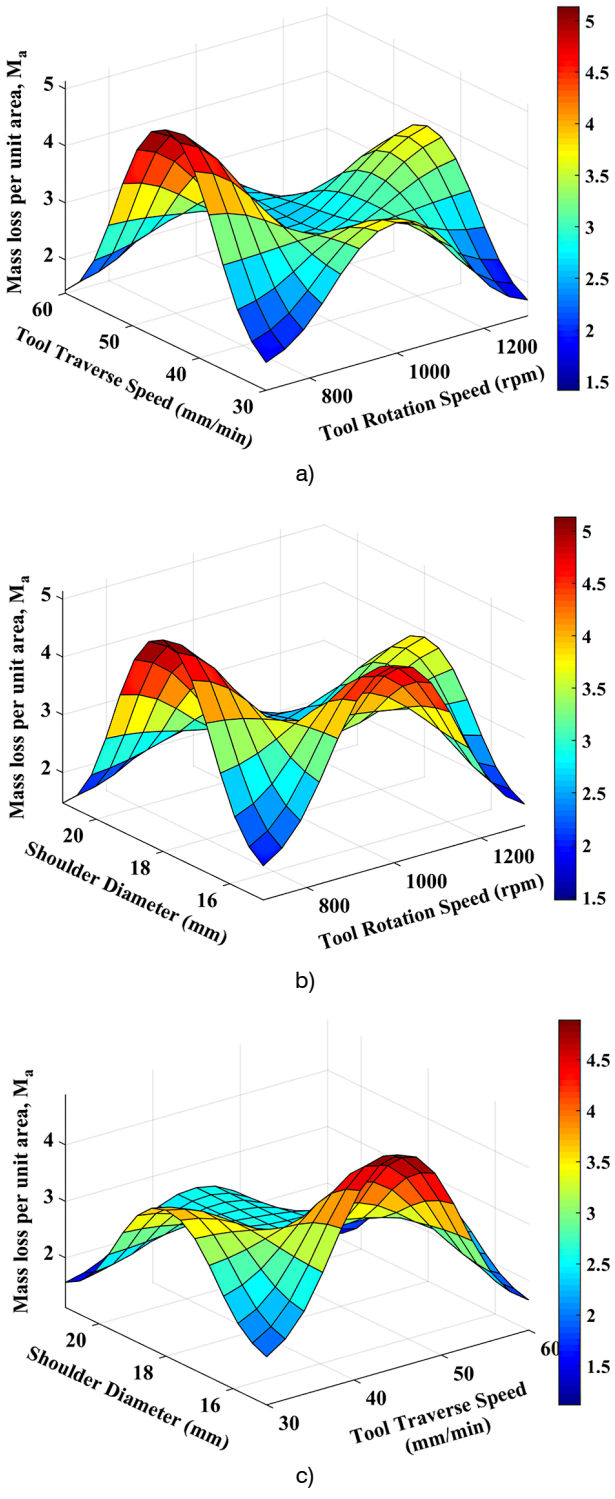

Fig. 11. Interaction effect of: a) TRS and TTS; b) TRS and SD; c) TTS and SD on M_a
Obr. 11. Vliv jednotlivých parametrů

CONCLUSION

Aluminum alloy AA5083 plates were friction stir processed by varying the process parameters and the intergranular corrosion susceptibility of the processed plates was assessed by conducting nitric acid mass loss test. The base specimen exhibited the highest mass loss of 19.967 mg cm^{-2} indicating high susceptibility to intergranular corrosion. The FSPed specimens exhibited a lower mass loss (less than 5 mg cm^{-2}) and were lesser prone to intergranular corrosion than the base material.

Mass loss of the specimens was predicted using Artificial Neural Network model, Mamdani's fuzzy inference system, and Sugeno fuzzy inference system. The Sugeno fuzzy system had the least percentage error in prediction (less than 10%) for all observations. The results indicate that friction stir processing process parameters significantly influence the intergranular corrosion resistance of AA5083 alloy.

REFERENCES

1. P. Cabot, F. Centellas, E. Perez, and R. Loukili, "Pitting and repassivation processes of Al · Zn · Mg alloys in chloride solutions containing sulphate," *Electrochimica acta* **1993**, 38 (18), 2741-2748.
2. J. C. Bailey, F. C. Porter, A. W. Pearson, and R. A. Jarman, "4.1 – Aluminium and Aluminium Alloys," *Corrosion (3rd Edition)*, pp. 4:3-3:37, Oxford: Butterworth-Heinemann, 1994.
3. J. A. Lyndon, R. K. Gupta, M. A. Gibson, and N. Birbilis, "Electrochemical behaviour of the β-phase intermetallic (Mg2Al3) as a function of pH as relevant to corrosion of aluminium–magnesium alloys," *Corrosion Science* **2013**, 70, 290-293.
4. R. H. Jones, V. Y. Gertsman, J. S. Vetrano, and C. F. Windisch Jr, "Crack-particle interactions during intergranular stress corrosion of AA5083 as observed by cross-section transmission electron microscopy," *Scripta Materialia* **2004**, 50 (10), 1355-1359.
5. E. Brillas, P. L. Cabot, F. Centellas, J. A. Garrido, E. Pérez, and R. M. Rodríguez, "Electrochemical oxidation of high-purity and homogeneous Al–Mg alloys with low Mg contents," *Electrochimica Acta* **1998**, 43 (7), 799-812.

6. R. S. Mishra, P. S. De, and N. Kumar, "Fundamental Physical Metallurgy Background for FSW/P," *Friction Stir Welding and Processing: Science and Engineering*, pp. 59-93, Cham: Springer International Publishing, 2014.
7. R. S. Mishra, and Z. Ma, "Friction stir welding and processing," *Materials Science and Engineering: R: Reports* **2005**, 50 (1), 1-78.
8. R. Padmanaban, V. Balusamy, and V. R. Kishore, "Effect of axial pressure and tool rotation speed on temperature distribution during dissimilar friction stir welding," *Advanced Materials Research* **2012**, 1934-1938.
9. R. V. Vignesh, R. Padmanaban, M. Arivarasu, S. Thirumalini, J. Gokulachandran, and R. Mutyala Sesha Satya Sai, "Numerical modelling of thermal phenomenon in friction stir welding of aluminum plates," *IOP Conference Series: Materials Science and Engineering* **2016**, 149 (1), pp. 012208.
10. Z. Ma, "Friction stir processing technology: a review," *Metallurgical and Materials Transactions A* **2008**, 39 (3), 642-658.
11. R. Padmanaban, R. Vaira Vignesh, M. Arivarasu, K. P. Karthick, and A. Abirama Sundar, "Process parameters effect on the strength of Friction Stir Spot Welded AA6061," *ARPN Journal of Engineering and Applied Sciences* **2016**, 11 (9), 6030-6035.
12. V. V. Ramalingam, and P. Ramasamy, "Modelling Corrosion Behavior of Friction Stir Processed Aluminium Alloy 5083 Using Polynomial: Radial Basis Function," *Transactions of the Indian Institute of Metals* **2017**, 70 (10), 2575-2589.
13. S. Ilangovan, R. V. Vignesh, R. Padmanaban, and J. Gokulachandran, "Comparison of Statistical and Soft Computing Models for Predicting Hardness and Wear Rate of Cu–Ni–Sn Alloy," *Progress in Computing, Analytics and Networking*, pp. 559-571: Springer, 2018.
14. R. V. Vignesh, and R. Padmanaban, "Forecasting Tribological Properties of Wrought AZ91D Magnesium Alloy Using Soft Computing Model," *Russian Journal of Non-Ferrous Metals* **2018**, 59 (2), 135-141.
15. B. Yegnanarayana, *Artificial neural networks*: PHI Learning Pvt. Ltd., 2009.
16. S.-C. Wang, "Artificial neural network," *Interdisciplinary Computing in Java Programming*, pp. 81-100: Springer, 2003.
17. G. Klir, and B. Yuan, *Fuzzy sets and fuzzy logic*: Prentice Hall New Jersey, 1995.
18. S. Sivanandam, S. Sumathi, and S. Deepa, *Introduction to fuzzy logic using MATLAB*: Springer, 2007.
19. R. R. Yager, and L. A. Zadeh, *An introduction to fuzzy logic applications in intelligent systems*: Springer Science & Business Media, 2012.
20. G. F. V. Voort, *ASM Handbook Volume 9: Metallography and Microstructures*, pp. 1184: ASM International, 2004.
21. E. Pouillier, A. F. Gourgues, D. Tanguy, and E. P. Busso, "A study of intergranular fracture in an aluminium alloy due to hydrogen embrittlement," *International Journal of Plasticity* **2012**, 34, 139-153.
22. G. M. Scamans, N. J. H. Holroyd, and C. D. S. Tuck, "The role of magnesium segregation in the intergranular stress corrosion cracking of aluminium alloys," *Corrosion Science* **1987**, 27 (4), 329-347.
23. Y.-K. Yang, and T. Allen, "Direct visualization of β phase causing intergranular forms of corrosion in Al–Mg alloys," *Materials Characterization* **2013**, 80, 76-85.
24. S.-J. Kim, S.-J. Lee, J.-Y. Jeong, and K.-H. Kim, "Electrochemical characteristics of Al–Mg and Al–Mg–Si alloy in sea water," *Transactions of Nonferrous Metals Society of China* **2012**, 22 (S3), 881-886.
25. R. Padmanaban, V. Ratna Kishore, and V. Balusamy, "Numerical simulation of temperature distribution and material flow during friction stir welding of dissimilar aluminum alloys." *Procedia Engineering* **2014**, 97, 854-863.
26. R. Goswami, G. Spanos, P. S. Pao, and R. L. Holtz, "Precipitation behavior of the ß phase in Al-5083," *Materials Science and Engineering: A* **2010**, 527 (4–5), 1089-1095.
27. M. Mezbahul-Islam, A. O. Mostafa, and M. Medraj, "Essential Magnesium Alloys Binary Phase Diagrams and Their Thermochemical Data," *Journal of Materials* **2014**, 33.
28. C. Meng, D. Zhang, H. Cui, L. Zhuang, and J. Zhang, "Mechanical properties, intergranular corrosion behavior and microstructure of Zn modified Al–Mg alloys," *Journal of Alloys and Compounds* **2014**, 617, 925-932.